Journal of Power Sources 201 (2012) 72–80

Contents lists available at SciVerse ScienceDirect

Journal of Power Sources

journal homepage: www.elsevier.com/locate/jpowsour

Poly(benzimidazole)/silica-ethyl-phosphoric acid hybrid membranes for proton exchange membrane fuel cells

Hsiu-Li Lin[a,b], Tsung-Hsien Tang[a], Chih-Ren Hu[a], T. Leon Yu[a,b,*]

[a] Department of Chemical Engineering & Materials Science, Yuan Ze University, Chung-Li, Taoyuan 32003, Taiwan
[b] Fuel Cell Center, Yuan Ze University, Chung-Li, Taoyuan 32003, Taiwan

ARTICLE INFO

Article history:
Received 28 September 2011
Received in revised form 26 October 2011
Accepted 31 October 2011
Available online 6 November 2011

Keywords:
Poly(benzimidazole)
Silica phosphoric acid
Proton exchange membrane fuel cell

ABSTRACT

Poly(benzimidazole) (PBI) is one of the excellent candidates of proton exchange membranes for high temperature (150–200 °C) proton exchange membrane fuel cells (PEMFCs). When applying to PEMFCs, the PBI membrane is usually doped with phosphoric acid to improve its proton conductivity and therefore PEMFC performance. In this work, we modify the PBI membranes by hybridizing PBI with diethyl phosphate ethyl-triethoxysilane (DEPE-TEOS). The self crosslink reactions of the DEPE-TEOS molecules and the inter-crosslink reactions between DEPE-TEOS and PBI imidazole –NH groups are then proceeded in the hybrid membrane, leading to the formation of crosslinked silica-ethyl phosphoric acid (SiP) nano-particles either bonding or without bonding to PBI. We show the mechanical properties, proton conductivity, and PEMFC performance of the PBI membrane are improved by hybridizing it with SiP nano-particles.

1. Introduction

The proton exchange membrane fuel cells (PEMFCs) have been considered as one of the most promising clean energy technologies and suitable primary power sources for both transportation and stationary applications. Recently, increasing attention has been paid on high temperature PEMFCs (>100 °C) due to their faster electrode kinetics, greater tolerance to impurities in the fuel stream and easier water-thermal management [1,2]. Phosphoric acid doped polybenzimidazole (PBI/H_3PO_4) membranes have been intensively investigated and successfully used more than any other proton exchange membranes (PEMs) in high temperature PEMFCs [3]. As a polymeric material, PBI possesses good mechanical strength as well as high chemical and thermal stabilities [4]. Furthermore, PBI membranes are impermeable to methanol, and possess a nearly zero water drag coefficient [5].

Recently, inorganic/organic hybrid membranes have been created by incorporating various amounts of inorganic solids into organic polymers, which serve as the matrix component [6]. The advantage of incorporating hygroscopic inorganic particles (e.g., SiO_2, TiO_2, etc.) into the organic polymer membranes is that the homogeneously dispersed, hydrophilic, inorganic solids improve both the water management and proton conductivity of the membrane by improving the self-humidification of the membrane of the anode side, by the back-diffusion of water produced at the cathode [7], and/or reducing the electro-osmotic drag. In case the inorganic filler is also a solid proton conductor (e.g., zirconium phosphate, heteropolyacid, etc.), the proton conductivity can be improved [8,9]. The mechanical properties of the organic polymer membrane are also expected to improve when interaction between the inorganic and organic components is favored. The disadvantage of hybridizing inorganic solids with organic polymer membranes is that the dispersed inorganic solid particles are likely to lead to nonhomogeneous composite membranes with rather large agglomerates of inorganic particles, which restricts the lower limit of the hybrid membrane's thickness. Furthermore, the proton conduction pathway for most of the inorganic particles is across their surface rather than through their bulk and tends to increase with decreasing inorganic particle sizes. This particle size reduction can be achieved using an in situ method to form inorganic particles within the hybrid membranes [8–11].

Inorganic/PBI hybrid membranes have been prepared using zirconium phosphate [12], phosphotungstic acid [13], silicotungstic acid [12,14,15], boron phosphate [16], organically modified montmorillonite (m-MMT) [17], mesoporous silica (MCM-41) [18], imidazole-modified silica [18], and sulfonated silica [19]. After doping with phosphoric acid, these hybrid membranes have higher proton conductivity than the un-modified PBI membranes. Although most of these reports [12–14] demonstrated improved proton conductivity and mechanical properties upon incorporation of inorganic particles into the PBI membranes, they did not show fuel cell performance *i–V* datum. Therefore, the applicability

* Corresponding author at: Department of Chemical Engineering & Materials Science, Yuan Ze University, Chung-Li, Taoyuan 32003, Taiwan.
Tel.: +886 3 4638800x2553; fax: +886 3 4559373.
E-mail address: cetlyu@saturn.yzu.edu.tw (T.L. Yu).

0378-7753/$ – see front matter © 2011 Elsevier B.V. All rights reserved.
doi:10.1016/j.jpowsour.2011.10.110

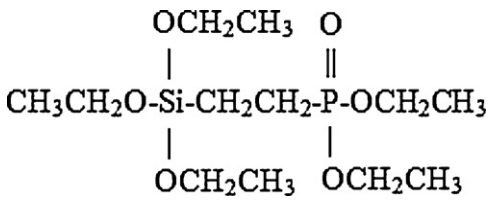

Fig. 1. The chemical structure of diethyl phosphate ethyl-triethoxyl silane (DEPE-TEOS).

of inorganic/PBI hybrid membranes to high temperature PEMFCs is still unclear.

Matsuda et al. [20,21] used the sol–gel method to prepare phosphosilicate gels from tetraethoxysilane (TEOS) with various kinds of phosphorus-containing compounds, such as phosphoric acid, triethyl phosphate, and diethyl phosphate ethyl-triethoxysilane (DEPE-TEOS), that showed high conductivities even under a dry atmosphere. Therefore these gels may be suitable for high-temperature, with low-humidity PEMFCs. In this work, we modified PBI membranes by hybridizing them with silica-ethyl-phosphoric acid (SiP) nano-particles using an in situ method. DEPE-TEOS (Fig. 1), which is composed of both silane and phosphate, was used as the modification compound to form the SiP particles in the PBI membranes by blending the polymer with various concentrations of DEPE-TEOS. The self-crosslinking of DEPE-TEOS and the inter-crosslinking between DEPE-TEOS and the imidazole >NH groups in PBI within the PBI/DEPE-TEOS blend led to the formation of crosslinked SiP both bonding and unbonding to the PBI molecules. We show that the mechanical properties, phosphoric acid doping level (PA_{dop}), and proton conductivity of the PBI membranes were improved. Thus, the PEMFC performance of the membrane electrode assembly (MEA) prepared using the PBI membrane was also improved when the membrane was hybridized with the SiP nano-particles.

2. Experimental

2.1. Synthesis of PBI

PBI was synthesized from 3,3′-diamino benzidine (Aldrich) and isophthalic acid (Aldrich) using polyphosphoric acid (Aldrich) as the solvent. The detailed polymerization procedure was same as those reported in the literature [22,23]. The molecular weight of the PBI was determined using a gel permeation chromatograph (GPC, Jasco PU-2080 plus) with an RI detector (Jasco RI-2031 plus). The mobile phase was N,N′-dimethyl acetamide (DMAc) mixed with 1.0 mg mL^{-1} of LiCl, and the concentration of PBI in the DMAc elution solution was 1.0 mg mL^{-1}. Another 1.0 mg mL^{-1} of LiCl was mixed with the elution solution to avoid aggregation of the PBI molecules via inter-imidazole hydrogen bonding [24]. The measurement was carried out at 40 °C with a flow rate of 0.8 mL min^{-1}. The average molecular weight obtained for PBI, using narrow molecular weight distribution polystyrene standard (Aldrich, $M_w/M_n \leq 1.1$) for calibration, was $<M_w> = 2.1 \times 10^5$ and $<M_n> = 9.3 \times 10^4$.

2.2. Preparation and characterizations of PBI–SiP hybrid membrane

2.2.1. Membrane preparations

A mixture of 2 g PBI and 48 g DMAc was stirred at 60 °C for 24 h. The DEPE-TEOS (Aldrich) was then mixed with the PBI/DMAc solution and stirred for another 1 h. Five PBI/DEPE-TEOS DMAc solutions that contained PBI/DEPE-TEOS wt/wt ratios of 1.0/0.0, 1.0/0.25, 1.0/0.5, 1.0/0.75, and 1.0/1.0 were prepared and were cast onto the glass plates using a doctor blade coater. The solvent of the cast films was dried at 80 °C for 1 h and then at 100 °C for 3 h. The cast membrane with a PBI/DEPE-TEOS wt ratio of 1.0/0.0 (i.e., pure PBI) was subsequently heated at 120 °C under vacuum for 6 h to obtain a pure PBI membrane. The other cast membranes, PBI/DEPE-TEOS wt ratios from 1.0/0.25 to 1.0/1.0, were heated at 120 °C under vacuum for another 1 h and then immersed in a 12 M HCl aqueous solution at 60 °C for 6 h to initiate hydrolysis, which led to the dissociation of the ethyl groups from both the diethylphosphate and triethoxysilane in DEPE-TEOS (Fig. 2, Eq. (1)). The membranes were then immersed in distilled water for 6 h, changing the water every 2 h to remove ethanol produced from the hydrolysis of DEPE-TEOS, and then dried at ambient environment. Subsequently, the membranes were heated at 120 °C under vacuum for 6 h to cause the silane inside the membranes to proceed with the self-crosslink reaction (Fig. 2, Eq. (2)) and the inter-crosslink reaction with the imidazole –NH groups of PBI (Fig. 2, Eq. (3)) and form the silica-ethyl-phosphoric acid (SiP) nano-particles [25,26]. These SiP nano-particles may or may not have been bonded to the PBI molecules as shown in the reaction scheme of Fig. 2. The membranes were then immersed in distilled water for 6 h, changing the water every 2 h to remove the residual HCl, and dried at ambient environment to obtain the PBI–SiP hybrid membranes. The designations, initial PBI/DEPE-TEOS wt ratios and final thicknesses of the pure PBI and four PBI–SiP hybrid membranes are listed in Table 1.

Table 1
The thicknesses (without doping phosphoric acid) and phosphoric acid doping levels of membranes.

Membrane	PBI/DEPE-TEOS (wt ratio)	Thickness (μm)	PA_{dop} (mol H_3PO_4/mol BI)
PBI	1/0	70 ± 1	6.3 ± 0.3
PBI–SiP-25	1/0.25	77 ± 1	6.9 ± 0.3
PBI–SiP-50	1/0.5	72 ± 2	7.3 ± 0.2
PBI–SiP-75	1/0.75	70 ± 2	8.6 ± 0.3
PBI–SiP-100	1/1	–	–

BI: a repeat unit of PBI.

2.2.2. Phosphoric acid doping level

The membranes prepared in Section 2.2.1 were doped with phosphoric acid by immersing then in an 85 wt% phosphoric acid aqueous solution at 70 °C for 72 h. The phosphoric acid doping level (PA_{dop}) of a PBI membrane is defined as the moles of phosphoric acid incorporated per mole of imidazole repeating unit and can be calculated using the following equation:

$$PA_{dop} = \frac{(W_1 - W_0)/98}{W_0/308} \quad (\text{mol } H_3PO_4\,(\text{mol PBI repeat unit})^{-1}) \quad (1)$$

where W_0 is the weight of the dry membrane, W_1 is the weight of the membrane doped with phosphoric acid, and the values 98 and 338 are the molecular weights of phosphoric acid and the imidazole repeating unit in PBI, respectively. To avoid the deviation due to moisture, before weighing, the membranes were dried by evaporating the water at 110 °C under vacuum for more than 3 h until an unchanged weight was obtained. The PA_{dop} data were averaged over three measurements.

2.2.3. Mechanical strength

The mechanical strength of the membranes was measured using an Instron testing machine (model 4204) in accordance with JIS-K7127. The data were averaged over five measurements.

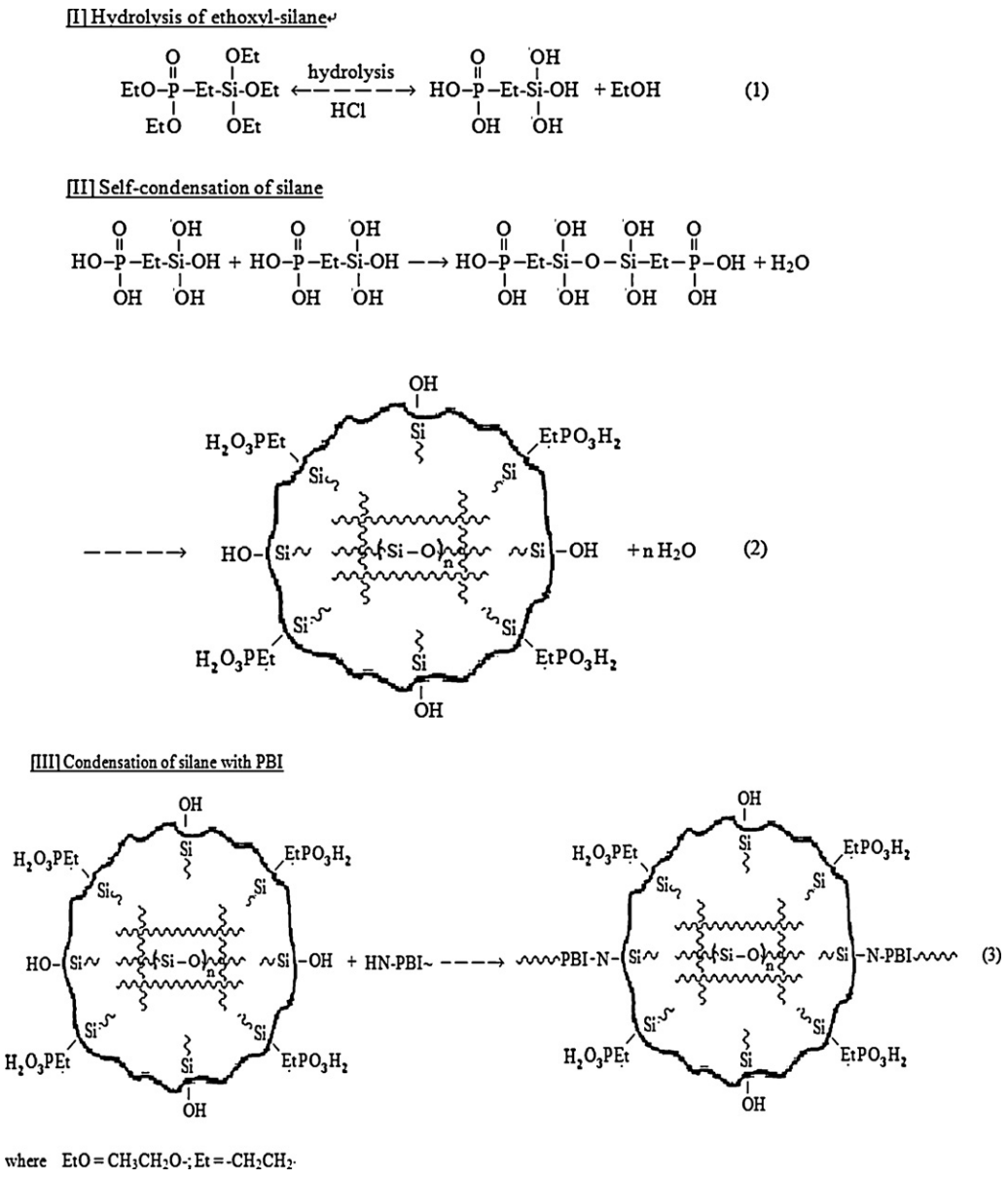

Fig. 2. Self reaction of DEPE-TEOS molecules and inter-crosslink reaction of silica–SiOH with PBI imidazole >NH group.

2.2.4. Conductivity measurement

The ionic conductivity (σ) was calculated from the measured current resistance (R) using Eq. (2):

$$\sigma = \frac{L}{A \times R} \tag{2}$$

where $A = 3.14\,\text{cm}^2$ is the cross-sectional area of the membrane for a resistance measurement and L is the thickness of the membrane for a given resistance measurement. R measurements were carried out by ac impedance spectroscopy using a Solartron 1260 gain phase analyzer interfaced to a Solartron 1480 multimeter. A device capable of holding the membranes during the R measurements was located between the probes. The testing device with a membrane was kept in a thermostat at the testing temperature with 0% RH under atmosphere for at least 3 h to allow the sample to reach an equilibrium state before the conductivity measurement was performed. These measurements were carried out at 140 °C, 160 °C, and 180 °C and took at least 2 h for the impedance spectroscopy to reach an equilibrium value. Each datum was the average of three measurements.

2.2.5. Thermal gravimetric analysis (TGA)

The TGA of membranes without doping with phosphoric acid was performed under N_2 gas using a Thermal Analysis (TA) model Q50 TGA, and a sample size of approximately 5–10 mg. Before TGA observations, the surface of each sample was dried with lens paper to remove the residual water from the surface of the membrane. The heating rate was 5 °C min^{-1} and the N_2 flow rate was 20 mL min^{-1}.

2.2.6. Scanning electron microscopy (SEM)

A scanning electron microscope (model JSM-5600, Jeol Co., Japan) was used to investigate the morphology of the surfaces of the membranes. The samples were coated with gold powder under vacuum before the SEM observations.

2.2.7. Energy dispersion X-ray (EDX) analysis

The membranes without swelling with phosphoric acid were used for EDX (model JSM-5600, Jeol Co., Japan) investigations.

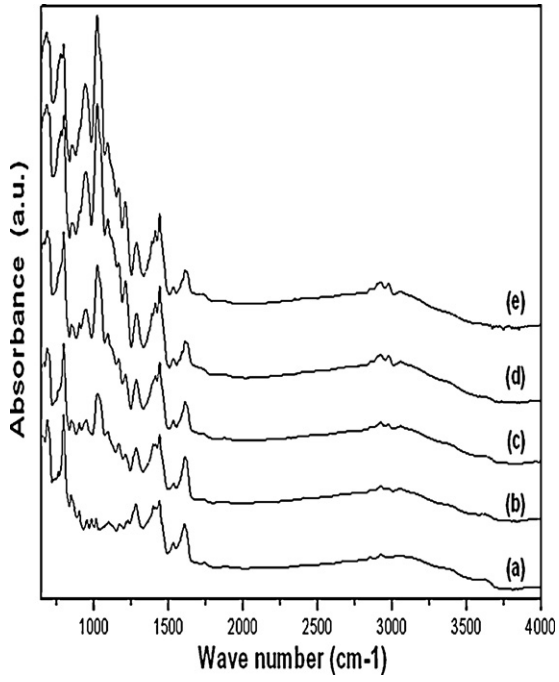

Fig. 3. FTIR spectra of PBI and PBI–SiP hybrid membranes. (a) PBI; (b) PBI–SiP-25; (c) PBI–SiP-50; (d) PBI–SiP-75; (e) PBI–SiP-100.

2.2.8. Transmission electron microscopy (TEM)

A transmission electron microscope (model JEM-2100, Jeol Co., Japan) operating at 80 kV was used to investigate the nano-morphology of the membranes.

2.3. PEMFC unit cell tests

The PBI and the PBI–SiP hybrid membranes doped with phosphoric acid were used to prepare MEAs. The catalyst was carbon supported Pt catalyst (Pt-C, with 40 wt% Pt, E-Tek Co). The Pt loadings at both the anode and cathode were 0.5 mg cm^{-2}. Pt-C/PBI/DMAc (3.5/1/49 by wt) catalyst solution was prepared by ultrasonic disturbance for 5 h. The catalyst solution was coated onto a carbon paper (SGL, 35BC) using an ultrasonic spray. Two sheets of carbon paper coated with a layer of the catalyst were placed on both sides of a membrane and pressed at 130 °C with a pressure of 50 N cm^{-2} for 3 min to obtain an MEA. The unit cell performance of each MEA was tested at 160 °C under ambient pressure using a FC5100 fuel cell testing system (CHINO Inc., Japan). Both the anode, H_2, and cathode, O_2, input flow rates were 200 mL min^{-1}. The active area of each MEA was 3.5 cm × 3.5 cm.

3. Results and discussion

3.1. FTIR studies of PBI and PBI–SiP hybrid membranes

Fig. 3 shows the FTIR spectra of the PBI, PBI–SiP-25, PBI–SiP-50, PBI–SiP-75, and PBI–SiP-100 membranes, which were prepared from the PBI/DEPE-TEOS blends with PBI/DEPE-TEOS wt ratios of 1.0/0.0, 1.0/0.25, 1.0/0.5, 1.0/0.75, and 1.0/1.0, respectively. By comparing the FTIR spectra of the PBI–SiP hybrids to that of PBI, we found two absorption peaks at 952 cm^{-1} and 1033 cm^{-1} corresponding to the Si–O stretching in silica [25,27] and an absorption peak at approximately 2930 cm^{-1} corresponding to C–H stretching in the ethyl group. These peaks increased with increasing SiP content of the PBI–SiP hybrid membranes. The N–H bending peak at approximately 1630 cm^{-1} for the PBI–SiP hybrid membranes was found to decrease with increasing SiP content, which suggests a decrease in the number of N–H groups due to the crosslinking of the imidazole >N–H with –Si–OH to form imidazole–silica, i.e., >N–Si–, bonds (Fig. 2, Eq. (3)). These results are indicative of the presence of SiP particles in the PBI–SiP hybrid membranes and the formation of >N–Si– bonds.

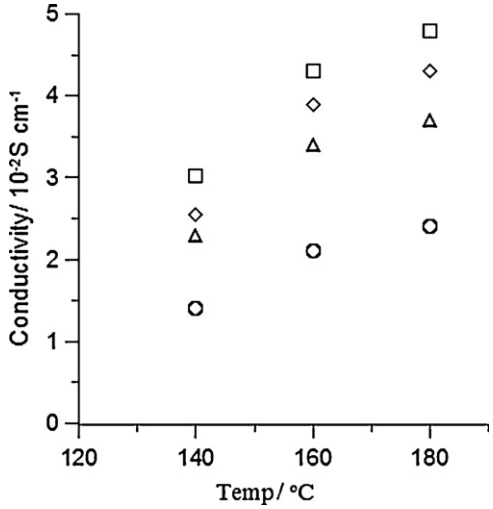

Fig. 4. Conductivities of membranes at 140 °C, 160 °C, and 180 °C with 0%RH. (○) PBI; (△) PBI–SiP-25; (◊) PBI–SiP-50; (□) PBI–SiP-75. Each datum was the average of three measurements with the error less than <7.0%.

3.2. Phosphoric acid doping level and proton conductivity

The thickness (before doping with phosphoric acid) and PA_{dop} of the PBI and PBI–SiP hybrid membranes are summarized in Table 1. The PA_{dop} of these membranes increased when the wt ratio of PBI/DEPE-TEOS varied from 1.0/0.0 to 1.0/0.75. However, when the DEPE-TEOS content was increased to a PBI/DEPE-TEOS wt ratio of 1.0/1.0 (i.e. PBI–SiP-100), the hybrid membrane dissolved during immersion in the 85 wt% phosphoric acid aqueous solution at 70 °C. Moreover, no PA_{dop} or σ measurement was carried out for the PBI–SiP-100 membrane. The dissolution of the PBI–SiP-100 membrane in the 85 wt% phosphoric acid aqueous solution can be attributed to the high disruption of hydrogen bonding between the imidazole >NH and –N=C– in the PBI membranes by the hybridizing of a large quantity of the SiP in the membrane. As will be shown in Section 3.3, the mechanical property data indicate the PBI–SiP-100 membrane is brittle (i.e., low strain). This poor mechanical property could be the reason that the PBI–SiP-100 membrane dissolved so easily in the 85 wt% phosphoric acid aqueous solution.

Fig. 4 shows the σ values for the membranes obtained at 140 °C, 160 °C, and 180 °C with 0% RH. These data show that the σ values increase with increasing either the SiP content or temperature of the membrane and had a PBI/DEPE-TEOS wt ratio dependency similar to PA_{dop}, which indicates a strong dependency of σ on PA_{dop}. Similar acid doping level and temperature dependencies of σ had also been observed for the acid-impregnated silica gels [20]. Though the phosphoric acid groups of the SiP particles are helpful for the proton transference in the membrane, however, the major contribution to the σ of the H_3PO_4 doped PBI–SiP membranes is the excess free H_3PO_4 molecules which are unbound to the imidazole groups of the PBI. It is known that the interaction between H_3PO_4 and the imidazole group (i.e., H_2PO_3–O–H···–N=C-PBI) allows PBI to retain H_3PO_4 and causes the protonation of the PBI. On the basis of IR analyses, Glipa et al. [28] and Bouchet et al. [29] suggested that the maximum degree of the H_3PO_4 interaction with the PBI imidazole group is two H_3PO_4 molecules per PBI repeating unit. When $PA_{dop} > 2$, excess free H_3PO_4 exists in the membranes.

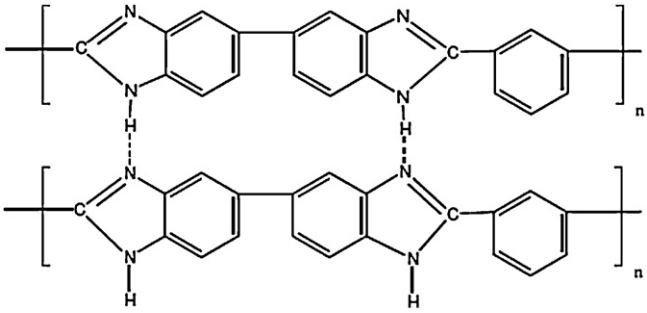

Fig. 5. Hydrogen bonds between imidazole –N–H···–N=C– groups.

It has been suggested by Ma et al. [30] that when $2 < PA_{dop} < 3$, there is little excess H_3PO_4 and the average $H_2PO_4^-\cdots H_3PO_4$ distance is larger than the imidazole >NH···–N=C– distance, and the proton conductivity in the acid-doped PBI results from the cooperative motion of two protons along the polymer-anion chain via the Grotthuss mechanism (see Fig. 2c of Ref. [30]). With increasing the doping level to $PA_{dop} > 3$, there is more excess free H_3PO_4, and the protons migrate, via the vehicle mechanism, along the mixed $H_2PO_4^-\cdots H_3PO_4$ and $H_2PO_4^-\cdots{}^+H$–N=C– anionic chains through successive proton transfer and anion reorientation steps (see Fig. 2d of Ref. [30]). From a proton conducting point of view, the acid molecules bound to the imidazole groups and the acidic anions bound both to the imidazole groups and the silica particles contribute to the proton conductivity only via the Grotthus mechanism, whereas the presence of the unbound $H_2PO_4^-$ ions is essential for the vehicle mechanism, but participates as well in the Grotthus mechanism [31]. From Table 1, we know that all the membranes had a PA_{dop} value larger than 2. Increasing the SiP content in the PBI–SiP hybrid membranes increases the PA_{dop} and thus increases the free excess H_3PO_4 and decreases the $H_2PO_4^-\cdots H_3PO_4$ distance, which facilitates proton transfer via the vehicle mechanism. Based on the IR analyses of solid PBI and PBI in the dilute LiCl/DMAc solution, Lin et al. [24] demonstrated strong hydrogen bonding between the imidazole –N–H and –N=C– groups in PBI (Fig. 5) that may retard the interaction of H_3PO_4 with the imidazole –N=C– groups. The increase in the PA_{dop} with increasing SiP content in the PBI–SiP hybrid membrane can be attributed to the disruption of the –N–H···N=C– hydrogen bonding by the SiP. This disruption of the –N–H···N=C– hydrogen bonding favors the H_2PO_3–O–H···–N=C–imidazole interactions and leads to the incorporation of the excess free H_3PO_4 into the PBI–SiP hybrid membranes.

3.3. Mechanical properties of membranes

The tensile stress, tensile strain, and Young's modulus of the PBI and the PBI–SiP hybrid membranes were measured at room temperature with a humidity of around 40–45% RH and are summarized in Table 2. The Young's modulus and tensile stress at break of the PBI–SiP hybrid membranes increased as the PBI/DEPE-TEOS wt ratio for preparing hybrid membranes was varied from 1.0/0.0 (i.e., PBI) to 1.0/0.75 (i.e., PBI–SiP-75) and then decreased as the PBI/DEPE-TEOS wt ratio for preparing the hybrid membranes was varied from 1.0/0.75 to 1.0/1.0 (i.e., PBI–SiP-100). The tensile strain of the PBI–SiP-25 and PBI–SiP-50 hybrid membranes was higher than that of the PBI membrane. The strain of the PBI–SiP hybrid membranes increased as the PBI/DEPE-TEOS wt ratio used to prepare the hybrid membranes was varied from 1.0/0.0 to 1.0/0.25 (i.e., PBI–SiP-25) and then decreased as it varied from 1.0/0.25 to 1.0/1.0. These results suggest that hybridizing a small amount of the SiP in the PBI membrane (PBI/DEPE-TEOS = 1.0/0.25 to 1.0/0.5 by wt) improved their toughness. However, as the DEPE-TEOS content for preparing PBI–SiP hybrid membrane increased to a PBI/DEPE-TEOS wt ratio closer to ~1.0/1.0, the PBI–SiP hybrid membrane became brittle because of the high content of crosslinked silica particles.

Table 2
Mechanical properties of membranes (Temp. 25 °C and 40–45%RH).

Membrane	Strain at break (%)	Young's modulus (GPa)	Stress at break (10 MPa)
PBI	5.5 ± 0.3	2.33 ± 0.18	6.61 ± 0.51
PBI–SiP-25	7.1 ± 0.4	2.36 ± 0.21	7.02 ± 0.63
PBI–SiP-50	6.4 ± 0.4	2.55 ± 0.20	7.21 ± 0.65
PBI–SiP-75	2.8 ± 0.2	3.00 ± 0.22	7.44 ± 0.59
PBI–SiP-100	0.6 ± 0.1	2.33 ± 0.18	7.26 ± 0.60

Inter-polymer PBI imidazole, >NH···–N=C–, hydrogen bonds (Fig. 5), PBI-imidazole –C=N–···H_2O_3P–C_2H_4–silica Lewis acid–base crosslink interactions, and the concentration of the crosslinked SiP nano-particles are the three key factors that control the mechanical properties of the PBI–SiP hybrid membranes. In these membranes, the SiP inorganic nano-particles behave as a filler for the PBI–SiP hybrid membranes and the PBI acts as a binder among the SiP inorganic particles. The filler behavior of the SiP particles and the Lewis acid-base crosslink interactions between PBI-imidazole –C=N– and H_2O_3P–C_2H_4–silica improved the tensile stress and modulus of the hybrid membranes when the PBI/DEPE-TEOS wt ratio was changed from 1.0/0 to 1.0/0.75. However, hybridizing the SiP nano-particles in the PBI membranes also disrupts the PBI imidazole –N–H···N=C– hydrogen bonding, which decreases both the tensile stress and modulus of the hybrid membranes when the PBI/DEPE-TEOS wt ratio for preparing PBI/SiP hybrid membranes was varied from 1.0/0.75 to 1.0/1.0. Another reason for the lower tensile stress and modulus of the PBI–SiP-100 hybrid membrane is the weaker binding forces among the SiP nano-particles caused by the lower PBI binder content. The –Et-PO_3H_2 side chains in the SiP nano-particles (Fig. 2, Eqs. (2) and (3)) and the disruption of the PBI imidazole –N–H···N=C– hydrogen bonding increased the polymer's free volume when the PBI membrane was hybridized with SiP. The higher strain in the PBI–SiP-25 and the PBI–SiP-50 hybrid membranes compared to the PBI membrane can be attributed to their higher free volume and adequate quantities of PBI-imidazole –C=N-···H_2O_3P–C_2H_4–silica Lewis acid–base crosslinks. The lower strains in PBI–SiP-75 and PBI–SiP-100 can be attributed to their higher concentration of the rigid inorganic SiP particles and lower PBI binder content, which results in weaker a binding force among the SiP nano-particles, and thus lowering the strain.

3.4. TGA study of PBI–SiP hybrid membranes

Fig. 6 shows the TGA curves of the PBI, PBI–SiP-25, PBI–SiP-50, and PBI–SiP-75 hybrid membranes without phosphoric acid doping. Because of its poor mechanical properties, the TGA of PBI–SiP-100 was not performed; therefore, its TGA curve is not shown in Fig. 6. The TGA data showed that these four membranes had similar weight losses as the temperature was raised from room temperature to ~420 °C. The weight loss below 300 °C can be attributed to the evaporation of moisture absorbed in the membranes. As the temperature was raised from 300 °C to ~450 °C, the membranes started to decompose. The weight loss curves of these four membranes were similar over this temperature range, which suggests that the weight loss primarily resulted from the decomposition of the PBI imidazole groups. As the temperature was raised from ~420 °C to ~530 °C, there was no significant weight loss for the PBI membrane. However, the TGA curves showed larger weight losses for the PBI–SiP hybrid membranes that increased with increasing SiP content. This weight loss can be attributed to

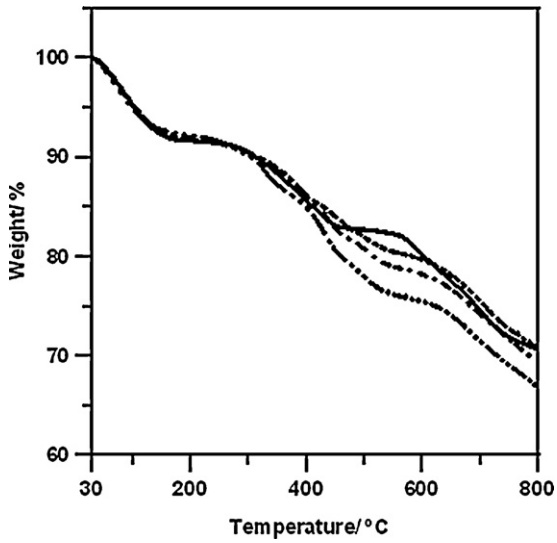

Fig. 6. TGA curves of membranes without doping H_3PO_4. (—) PBI; (--) PBI–SiP-25; (—·) PBI–SiP-50; (—···) PBI–SiP-75. The heating rate was 5 °C min^{-1} and the N_2 flow rate was 20 mL min^{-1}.

the decompositions of both the ethyl-PO_3H groups in the silica–Et-PO_3H (Fig. 2, Eqs. (2) and (3)) and the >N–Si– groups in the imidazole >N–Si–silica (Fig. 2, Eq. (3)). The TGA curves showed a plateau regime in the temperature region between ~450 °C and ~560 °C for the PBI membrane and ~530 °C to ~620 °C for the PBI–SiP hybrid membranes. As the temperature was raised above ~620 °C, the rates of weight loss for these four membranes were similar, suggesting that the decomposition of the PBI main chain occurred in this temperature region. As the working temperature of PBI and PBI–SiP membranes in PEMFCs is approximately 140–200 °C, which is approximately 100 °C lower than their decomposition temperature, the PBI–SiP hybrid membranes are suitable for high-temperature PEMFCs.

3.5. SEM and EDX studies of PBI–SiP hybrid membrane

The morphology of the PBI–SiP hybrid membranes was investigated using SEM and EDX. The SEM micrographs in Fig. 7 show that the plane surface of the PBI–SiP-75 hybrid membrane is smooth. Fig. 8a, b, c, and d are the EDX graphs of C, N, Si, and P elemental analyses, respectively, of the plane surface of the PBI–SiP-75 hybrid membrane. The bright spots in each EDX graph corresponds to the element being analyzed show a homogeneous distribution of the C, N, Si, and P elements in the plane surface. Similar SEM and

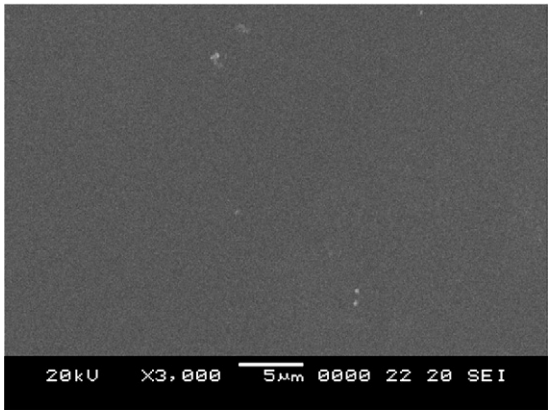

Fig. 7. SEM (3000×) of the plane surface of the PBI–SiP-75 hybrid membrane.

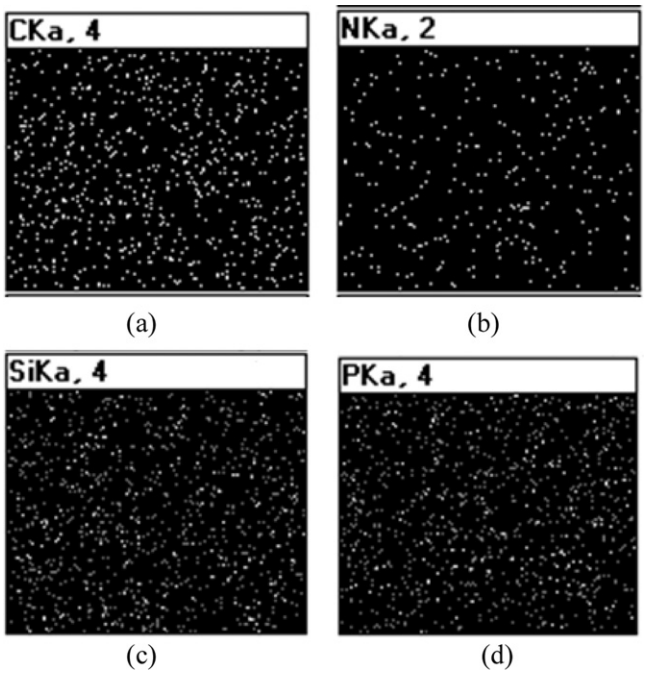

Fig. 8. EDX C, N, Si, P-mapping of the plane surface of the PBI–SiP-75 hybrid membrane. (a) Carbon element; (b) nitrogen element; (c) silicon element; (d) phosphorus element. The bright spots in each mapping graph indicate the element of EDX analysis.

EDX observations were also obtained from a cross section of the PBI–SiP-75 hybrid membrane and indicated no agglomeration of SiP particles formed. The SEM and the EDX graphs of the PBI–SiP-25 and PBI–SiP-50 hybrid membranes, which contain fewer SiP particles than the PBI–SiP-75 hybrid membrane, also had smooth surfaces and homogeneous distributions of C, N, Si, and P elements both on the plane surface and in the cross section and are not shown here.

3.6. TEM studies of PBI–SiP hybrid membrane

The morphology of the PBI–SiP hybrid membranes was studied further using a high-resolution TEM. Fig. 9a and b shows the TEM micrographs of the pure PBI and PBI–SiP-75 hybrid membranes, respectively. Careful investigating these two micrographs, we observed bright spots dispersing in the PBI–SiP-75 membrane (Fig. 9b), but no bright spot was observed in the pure PBI membrane (Fig. 9a). The TEM micrograph of the PBI–SiP-75 membrane shows that the Si–P particles are homogeneously distributed, with no observed agglomeration, in the hybrid membrane with particle sizes of approximately 1 nm, which is consistent with the SEM and EDX observations discussed in Section 3.5. In the hybrid membrane, DEPE-TEOS is a minor component dispersing in the PBI matrix. The competition between the self-crosslinking of the DEPE-TEOS molecules (Fig. 2, Eq. (2)) and the inter-crosslinking of the DEPE-TEOS molecules with PBI imidazole >NH groups (Fig. 2, Eq. (3)) caused the formation and the homogenous distribution of the small Si–P nano-particles in the PBI–SiP hybrid membranes. From the TEM, SEM, and EDX observations, we may conclude a homogeneous distribution of SiP nano-particles in the hybrid membranes was prepared using the in situ method.

3.7. PEMFC performance tests

To evaluate their performance in fuel cells, PBI and PBI–SiP-25, PBI–SiP-50, PBI–SiP-75 hybrid membranes were used to make

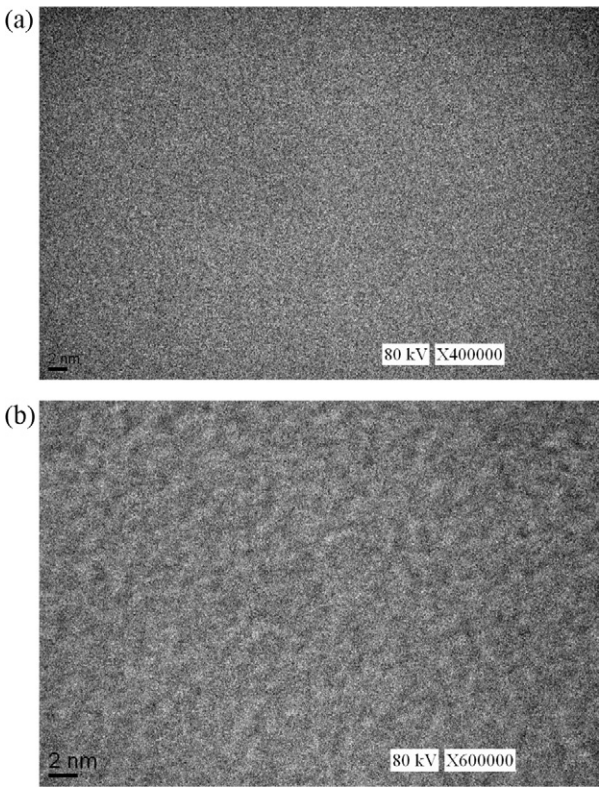

Fig. 9. TEM micrographs of the membranes. (a) Pure PBI membrane and (b) PBI–SiP-75 hybrid membrane. The scale bar at the bottom left hand side is 2 nm. The bright spots in (b) indicate the silica-ethyl phosphoric acid particles.

MEAs, that were tested for PEMFC unit cell performance at 160 °C under ambient pressure. Fig. 10 shows the *i–V* curves and Table 3 summarizes the PEMFC open circuit voltages (OCVs) and maximum power densities (PD_{max}s) of these MEAs. All of the MEAs had OCV values higher than 0.90 V, which indicates low fuel penetration across the membrane [32]. From the *i–V* curves and the PD_{max} data, we found that PBI–SiP-25 performed similarly to PBI in the fuel cell.

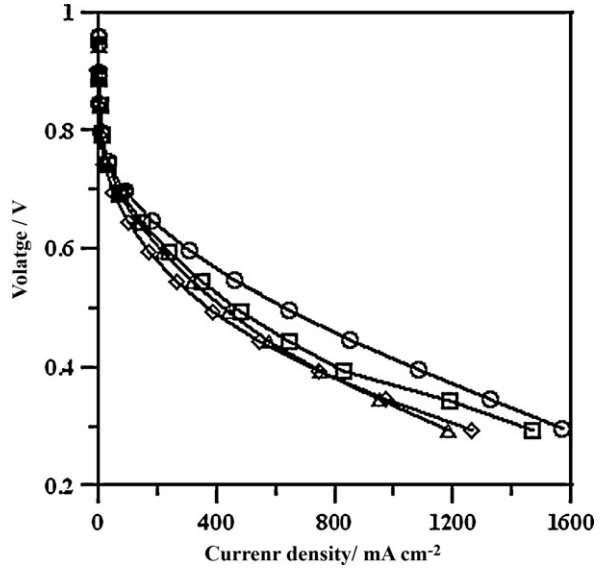

Fig. 10. PEMFC unit cell test *i–V* curves obtained at 160 °C and ambient pressure with unhumidified H_2/O_2 flow rates of 200 mL min^{-1}. MEA active area 3.5 cm × 3.5 cm, and Pt loadings were 0.5 mg cm^{-2} both at anode and cathode. Membranes for preparing MEAs: (◊) PBI; (△) PBI–SiP-25; (□) PBI–SiP-50; (○) PBI–SiP-75.

Table 3
PEMFC unit cell test OCV and PD_{max} data.

Membrane	OCV (V)	PD_{max} (mW cm^{-2})
PBI	0.94	368
PBI–SiP-25	0.94	344
PBI–SiP-50	0.95	432
PBI–SiP-75	0.96	465

However, the PBI–SiP-50 and the PBI–SiP-75 hybrid membranes performed better in the fuel cell than the pure PBI membrane. These results were consistent with the membrane PA_{dop} data (Table 1) and σ data (Fig. 4), which demonstrated that the PA_{dop} and σ of the hybrid membranes increased with increasing the SiP content up to the PBI–SiP-75 membrane. As discussed in Section 3.2, it is the PA_{dop}, rather than the SiP content, dominates the σ and thus the PEMFC performance of the PBI–SiP hybrid membrane. The hybridizing of the SiP in a PBI membrane facilitates the swelling of the phosphoric acid and increases the free H_3PO_4 content in the membrane. However, the introduction of the free H_3PO_4 in the PBI membrane also causes the separation of the hydrogen bonding between the nitrogen atoms of PBI backbones leading to a decrease in the tensile strength or modulus of the membrane. It had been suggested that a practical PA_{dop} of a PBI membrane for PEMFC application should take into account both the conductivity and mechanical strength of the membrane, which are opposite functions of the PA_{dop} [31]. A high mechanical strength membrane, such as PBI with a high molecular weight [33] or with a suitable crosslinkage [34,35], can be allowed to a high PA_{dop} with proper mechanical strength for PEMFC applications [31]. In Table 2, we show that both the tensile stress and modulus of the PBI membrane are improved by hybridizing SiP in the membrane with a SiP/PBI wt ratio ranging from 0.25 to 0.75. The better mechanical strength for the PBI–SiP membrane than the pure PBI membrane could be one of the reasons that the PBI–SiP membrane has a higher PA_{dop} and thus a better fuel cell performance than pure PBI membrane.

3.8. PEMFC 300 h continuous performance test

The result of the 300 h lifetime test of the PBI–SiP-75 unit cell, which operated at 160 °C with a constant current density $i = 200\ mA\ cm^{-2}$ is shown in Fig. 11. During the initial 36 h test, the cell voltage increased from 0.627 V to 0.631 V; however, the voltage decayed from 0.631 V to 0.619 V between 40 h and 144 h then fluctuated around 0.619 V from 144 h to 300 h. The estimated voltage decay rate between 36 h and 300 h was approximately $4.55 \times 10^{-5}\ V\ h^{-1}$. Several researchers have reported long lifetime tests of PBI-based high-temperature PEMFCs [36–40]. During long-duration fuel cell tests under a fixed loading current, two regions were observed in the output voltage versus time curve. The first initial testing period, during which the cell voltage increased with operating time, was the "activation region" and was followed by the "decay region", during which the cell voltage decreased with operating time. Liu et al. [38], Hu et al. [36], and Zhai et al. [39] reported that the time length of the activation region was approximately 90–130 h for the PBI-based PEMFCs. The time length of the activation region for the PBI–SiP based PEMFC in this work was shorter than that of the PBI-based. Liu et al. [38] attributed the improvement in fuel cell performance at "activation region" to the better contact of the membrane with the catalyst layers due to the pressure from the end plates and expansion of the interface at high temperature. Lin et al. [40] carried out a continuous lifetime test of an H_3PO_4 doped PBI/porous PTFE (poly(tetra fluoroethylene)) composite MEA at 160 °C. The pH value of the cathode output water was measured during the continuous lifetime test and was found to be approximately 4.3–6.0 at the first 30 h and ~5.5–6.0 after 150 h

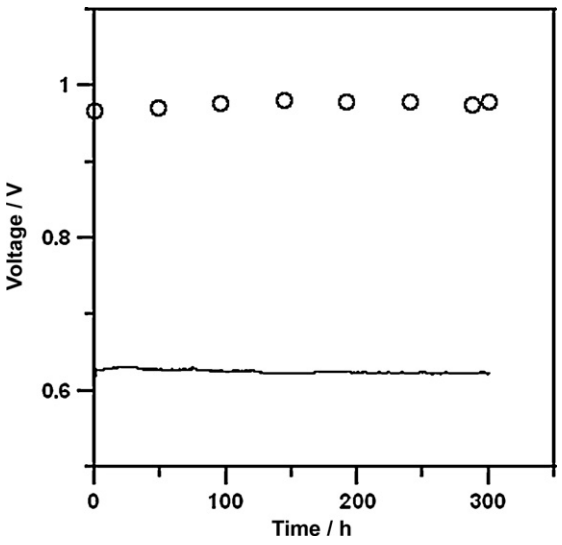

Fig. 11. Variations of OCV (○) and cell voltage (—) of PBI–SiP-75 MEA unit cell during a 300 h continuous operation at a constant current density $i = 200\,mA\,cm^{-2}$ under 160 °C and ambient pressure. Pt loadings were $0.5\,mg\,cm^{-2}$ for both anode and cathode; active area = 3.5 cm × 3.5 cm; unhumidified H_2/O_2 flow rates were $200\,mL\,min^{-1}$.

of the continuous lifetime test. They suggested that migration of excess phosphoric acid molecules which did not bound to the PBI imidazole from the MEA occurred during the first 30 h of the lifetime test. After most of the excess phosphoric acid molecules had migrated out of the MEA, the pH value of the cathode output water stabilized in a steady state and at a higher pH value than observed in the initial period of the lifetime test.

Fig. 12 shows the *i*–*V* polarization curves obtained at five testing times during the 300 h continuous lifetime test. The OCV data obtained from each *i*–*V* measurement were also plotted against life testing time and shown in Fig. 11. The OCV were approximately 0.96–0.98 V during the 300 h continuous lifetime test, which indicates a low fuel crossover of the membrane. The *i*–*V* data after 144 h showed that the current density at a cell potential of 0.3 V was lower than those at both the beginning of and 36 h into the lifetime test,

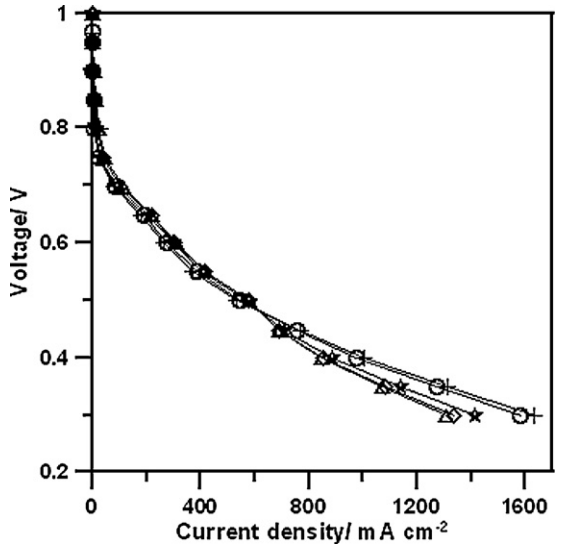

Fig. 12. *i*–V curves of PBI–SiP-75 MEA measured at (○) 0 h, (+) 36 h, (☆) 144 h, (◊) 240 h, and (△) 300 h during a 300 h continuous operation at a constant current density $i = 200\,mA\,min^{-1}$ and ambient pressure. Pt loadings: anode = $0.5\,mg\,cm^{-2}$, cathode = $0.5\,mg\,cm^{-2}$; active area = 3.5 cm × 3.5 cm; H_2/O_2 flow rates $200\,mL\,min^{-1}$.

which suggests that some of the gas flow pathways in the catalyst layers were blocked and the H_2 and O_2 molecules were not able to reach all of the catalyst particles. As suggested previously [40,41], the blockage of gas pathways in the catalyst layers could be due to the migration of phosphoric acid from the membrane to the cathode catalyst layer. This blockage of the H_2 and O_2 gas flows indicated a change in the catalyst layer morphology after long times at high temperatures.

4. Conclusions

The PBI–SiP hybrid membranes were prepared by blending DEPE-TEOS in PBI using an in situ method. The self-crosslinking reactions of the DEPE-TEOS molecules and the inter-crosslinking reactions between the DEPE-TEOS and the PBI imidazole –NH groups led to the formation of crosslinked SiP nano-particles both with and without binding to the PBI. We showed that the mechanical properties, proton conductivity, and PEMFC performance of the PBI membrane improved greatly when the initial wt ratio of PBI/DEPE-TEOS to prepare the PBI–SiP hybrid membranes was around 1.0/0.50 to 1.0/0.75. The 300-h continuous PEMFC lifetime test of the PBI–SiP-75-based MEA at 160 °C with a fixed $i = 200\,mA\,cm^{-2}$ showed a voltage decay rate of $4.55 \times 10^{-5}\,V\,h^{-1}$, which indicates the PBI–SiP hybrid membranes are relatively stable.

Acknowledgement

The authors would like to thank for the financial support by Bureau of Energy, Ministry of Economy Affair of Taiwan through grant 99-D0137-4.

References

[1] Q.F. Li, R.H. He, O.J. Jensen, N.J. Bjerrum, Chem. Mater. 15 (2003) 4896–4915.
[2] M.A. Hickner, H. Ghassemi, Y.S. Kim, B.R. Einsla, J.E. McGrath, Chem. Rev. 104 (10) (2004) 4587–4612.
[3] H. Vogel, C.S. Marvel, J. Polym. Sci. A: Polym. Chem. 34 (7) (1996) 1125–1153.
[4] Y.F. Zhai, H.M. Zhang, Y. Zhang, D.M. Xing, J. Power Sources 169 (2007) 259–264.
[5] D.F. Cheddie, N.D.H. Munroe, J. Power Sources 160 (2006) 215–223.
[6] D.J. Jones, J. Roziere, in: W. Vielstich, A. Lamm, H.A. Gasteiger (Eds.), Handbook of Fuel Cells, vol. 3, John Wiley & Sons, 2003 (Chapter 35).
[7] M. Watanabe, H. Uchida, E. Emori, J. Phys. Chem. B 102 (1998) 3129.
[8] H.L. Lin, T.J. Chang, J. Membr. Sci. 325 (2008) 880–886.
[9] H.L. Lin, S.H. Yeh, T.L. Yu, L.C. Chen, J. Polym. Res. 16 (2009) 519–527.
[10] R.V. Gummaraju, R.B. Moore, K.A. Mauritz, J. Polym. Sci. B: Polym. Phys. 34 (1996) 2383.
[11] W. Apichatachutapan, R.B. Moore, K.A. Mauritz, J. Appl. Polym. Sci. 62 (1996) 417.
[12] R.H. He, Q.F. Li, G. Xiao, N. Bjerrum, J. Membr. Sci. 226 (2003) 169–184.
[13] P. Staiti, M. Minutoli, S. Hocevar, J. Power Sources 90 (2000) 231–235.
[14] P. Staiti, M. Minutoli, J. Power Sources 94 (2000) 9–13.
[15] P. Staiti, Mater. Lett. 47 (2000) 241–246.
[16] S.M.J. Zaidi, Electrochim. Acta 50 (2005) 4771–4777.
[17] S.W. Chuang, S.L.C. Hsu, C.L. Hsu, J. Power Sources 168 (2007) 172–177.
[18] V. Kurdakova, E. Quartarone, P. Mustarelli, A. Magistris, E. Caponetti, M.L. Saladino, J. Power Sources 195 (2010) 7765–7769.
[19] Suryani, Y.L. Liu, J. Membr. Sci. 332 (2009) 121–128.
[20] A. Matsuda, Y. Nono, T. Kanzaki, K. Tadanaga, M. Tatsumisago, T. Minami, Solid State Ionics 145 (2001) 135–140.
[21] A. Matsuda, T. Kanzaki, K. Tadanaga, M. Tatsumisago, T. Minami, Solid State Ionics 145 (2001) 161–166.
[22] M. Ueda, M. Sato, A. Mochizuki, Macromolecules 18 (1985) 2723–2726.
[23] H.L. Lin, T.L. Yu, W.K. Chang, C.P. Cheng, C.R. Hu, G.B. Jung, J. Power Sources 164 (2007) 481–487.
[24] H.L. Lin, Y.C. Chen, C.C. Li, C.P. Cheng, T.L. Yu, J. Power Sources 181 (2008) 228–236.
[25] Q. Deng, R.B. Moore, K.A. Mauritz, J. Appl. Polym. Sci. 68 (1998) 747–763.
[26] S.K. Young, W.L. Jarrett, K.A. Mauritz, Polym. Eng. Sci. 41 (2001) 1529–1539.
[27] R.M. Silverstein, G.C. Bassler, T.C. Morrill, Spectrometric Identification of Organic Compounds, 4th ed., John Wiley & Sons, 1981 (Chapter 3).
[28] X. Glipa, B. Bonnet, D.J. Jones, J. Roziere, J. Mater. Chem. 9 (1999) 3045–3049.
[29] R. Bouchet, E. Siebert, Solid State Ionics 118 (1999) 287–299.
[30] Y.L. Ma, J.S. Wainright, M.H. Litt, R.F. Savinell, J. Electrochem. Soc. 151 (1) (2004) A8–A16.

[31] Q. Li, J.O. Jensen, R.F. Savinell, N.J. Bjerrum, Prog. Polym. Sci. 34 (2009) 449–477.
[32] J. Larminie, A. Dicks, Fuel Cell Systems Explained, John Wiley & Sons, 2000 (Chapter 3).
[33] J. Lobato, P. Canizares, M.A. Rodrigo, J.J. Linares, J.A. Aguilar, J. Membr. Sci. 306 (2007) 47–55.
[34] Q. Li, J.O. Jensen, C. Pan, V. Bandur, M. Nilsson, F. Schonberger, Fuel Cells 8 (2008) 188–199.
[35] Q. Li, C. Pan, J.O. Jensen, P. Noye, N.J. Bjerrum, Mater. Chem. 19 (2007) 350–352.
[36] J. Hu, H. Zhang, Y. Zhai, G. Liu, B. Yi, Int. J. Hydrogen Energy 31 (2006) 1855–1862.
[37] L. Xiao, H. Zhang, E. Scanlon, L.S. Ramanathan, E.W. Choe, D. Rogers, T. Apple, B. Benicwicz, Chem. Mater. 17 (2005) 5328–5333.
[38] G. Liu, H. Zhang, J. Hu, Y. Zhai, D. Xu, Z.G. Shao, J. Power Sources 162 (2006) 547–552.
[39] Y. Zhai, H. Zhang, G. Liu, J. Hu, B. Yi, J. Electrochem. Soc. 154 (1) (2007) B72–B76.
[40] H.L. Lin, Y.S. Hsieh, C.W. Chiu, T.L. Yu, L.C. Chen, J. Power Sources 193 (2009) 170–174.
[41] Y. Oono, A. Sounai, M. Hori, J. Power Sources 189 (2011) 943–949.